Computers & Geosciences 52 (2013) 437–442

Contents lists available at SciVerse ScienceDirect

Computers & Geosciences

journal homepage: www.elsevier.com/locate/cageo

Software review

Flexible, inversion-based Matlab implementation of the Radon transform

ARTICLE INFO

Keywords:
Inverse theory
Phase identification
Reflectivity structure
Seismic discontinuities
Signal processing
Spatial interpolation

ABSTRACT

This study reviews the theory, programming designs and merits of two new Matlab-based routines for the forward and inverse Radon transform. These routines offer users flexible choices of integration path functions to take advantage of improved Radon-domain identification and isolation of seismic phases. Least-squares inversion of frequency components and judicious choices of regularization techniques enables additional noise suppression and signal enhancement in the Radon domain. The forward Radon transform routine has the added benefit of spatial interpolation for irregularly sampled data. The accuracy and applicability of these two new routines are demonstrated using data sets containing long-period SS precursors and high-frequency receiver functions. With minimal modifications these two highly portable, carefully documented Radon-transform routines could be easily adapted for a broad range of applications.

1. Introduction

The Radon transform (from here on RT) was originally formulated as an integration of a 2D function along a set of straight lines expressed by orientation angles and distances to the origin (Radon, 1917). This problem has since been extended to more general functions and laid the foundation for applications in astrophysics (Bracewell, 1956), computed axial tomography (Cormack, 1963), seismic tomography (see Liu and Gu (in press) for review) and reflection seismology (Sacchi and Ulrych, 1995; Trad et al., 2003). More recently, earthquake-based seismic structure analysis also utilized RT in both traditional (An et al., 2007; Gu et al., 2009; Gu and Sacchi, 2009) and more generalized (Cao et al., 2010) forms. Within the context of seismology, the integration paths are typically constrained by ray parameter (alternatively called slowness and denoted by p), a conserved quantity along a potentially curved trajectory in a heterogeneous medium. Some applications may adopt the form

$$t = \tau + p\Delta, \tag{1}$$

where seismic arrival time (t) is linearly dependant on epicentral distance (Δ). The ability of RT to project move-out (spatial) data $M(t,\Delta)$ to the Radon domain $R(\tau,p)$ allows for the identification and differentiation of unique phase arrivals. Extraneous arrivals may be conveniently isolated and attenuated in the Radon domain. The forward operator can also be applied to a filtered Radon domain, effectively minimizing obfuscating phases in the spatial domain. This property has been instrumental in exploration seismology for the removal of multiple reflections (Thorson and Claerbout, 1985; Hampson, 1986; Beylkin, 1987). With the advent of increasingly dense regional seismic arrays (e.g., USArray and Hi-Net, Japan) as well as convenient access and dissemination of geophysical data, it is becoming more feasible to extend techniques such as RT to interrogate reflectivity structure at global or regional scales (An et al., 2007; Gu et al., 2009).

In this study we document the theory, implementation and usage of Radon_inverse and Radon_forward, two open-source Matlab-based routines. These functions have been designed under the premise of simplicity and flexibility, consistent with the built-in Matlab functions (e.g., fft and interp1). Radon_inverse implements a frequency-based inversion and includes regularization methods pertaining to ℓ_2 and ℓ_1 norms as well as a Cauchy-based (Sacchi and Ulrych, 1995) cost function. Both the forward and inverse routines include linear and parabolic path functions, and the ambitious user may incorporate additional path functions, regularizations or inversion techniques as needed. The routine's functionality has been tested on long-period shear wave reflections from mantle interfaces (e.g., Shearer and Masters, 1992) and high-frequency receiver functions (see Rondenay, 2009 for review). Our method and algorithm remain general and are easily adaptable to other applications, both within and outside of seismology.

2. Theory

RT represents an integral transform that in its original context described an integration along the lines parameterized by distance to the origin and angular orientation. This parameterization leads to Radon inversions commonly referred to as sinograms in computed axial tomography. In seismology, discrete approaches to this problem have been estimated using a summation known as slowness slant stacking. The equation governing the summation-based approximation to the Radon domain (vespagram) is expressible as

$$R(\tau_k,p_i) = (1/N_\Delta)\sum_{j=1}^{N_\Delta} M(\tau_k + T(p_i,\Delta_j,\delta),\Delta_j). \tag{2}$$

For each parameter of slowness p_i, a summation is performed over all seismograms with offsets/distances Δ_j in the move-out domain. Each seismogram is shifted in time by the function

http://dx.doi.org/10.1016/j.cageo.2012.08.013

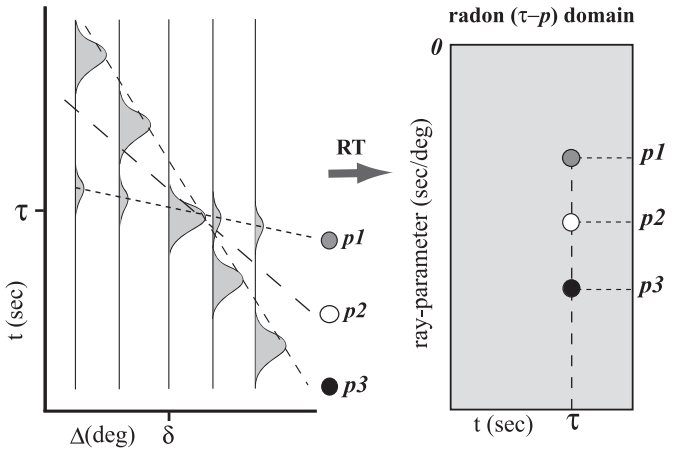

Fig. 1. A caricature depicting the Radon transform. Linear path-functions are focused around the distance parameter δ in the spatial domain (left panel). Integration paths defined by ray parameters p1, p2 and p3 intersect in the spatial domain at (τ,δ) (left panel), which are projected to the Radon domain as energy foci (right panel). Integration along ray parameter p3 maps the high-amplitude phase in the spatial domain to an energetic signal in the Radon domain (dark solid circle). A weaker Radon signal results from integrating along parameter p1 (gray circle, right panel), due to smaller amplitude phase move-out, while an integration path devoid of arrivals (see p2) yields minimal Radon energy (white circle). It should be noted that these three paths only intersect at the designated distance parameter δ, whereas any other choice would result in distinct τ arrivals in the Radon domain.

$T(p_i,\Delta_j,\delta)$ that describes the path of integration in the spatial domain. Coherent signals along these paths (see Fig. 1) will stack constructively and potentially increases signal-to-noise ratio by a factor of $\sqrt{N_\Delta}$ (Shearer, 1991), where N_Δ is the number of seismograms. Integration methods are distinguished by their path function as linear, parabolic, hyperbolic or generalized. In our path function formulation, a phase's intersection in time with the distance parameter δ determines the τ arrival in the Radon domain.

Slant stack methods (Rost and Thomas, 2009) offer a simple, effective technique to estimate the Radon domain. Other non-linear stacking techniques such as *N*-th root (Kanasewich et al., 1973) and phase-weighted (Schimmel and Paulssen, 1997) have been employed with slowness slants to detect coherent, low amplitude arrivals and increase slowness resolution. However, these alternatives tend to distort the signal's amplitude information, a potentially fatal flaw for some applications. Inversion-based methods have been suggested as a more robust and reliable approach (Beylkin, 1987; Sacchi and Ulrych, 1995). Formulating RT as an inverse problem requires the forward relationship between the spatial and Radon domains

$$M(t_k,\Delta_j)=\sum_{i=1}^{N_p} R(\tau_k-T(p_i,\Delta_j,\delta),p_i). \tag{3}$$

To condition Eq. (3) into a form that is conducive to inversion, we perform the Fourier transform

$$M(\omega_k,\Delta_j)=\sum_{i=1}^{N_p}\exp(-i\omega_k T(p_i,\Delta_j,\delta))R(\omega_k,p_i), \tag{4}$$

where the shift theorem modifies the discrete Radon equation into a more tractable form. For a single, constant frequency ω_k, this equation may be expressed in the matrix notation as

$$M(\Delta_j)=\mathbf{A}(\Delta_j,p_i)R(p_i), \tag{5}$$

and $\mathbf{A}(\Delta_j,p_i)$ denotes a matrix of time shifts with magnitudes determined by the path function (Sacchi and Ulrych, 1995; An et al., 2007; Gu and Sacchi, 2009). Alternative Radon methods based on spline convolution have been utilized in medical tomography (La Rivière and Pan, 1998; Horbelt et al., 2002). The use of the Fourier transform in our implementation enables a least-squares inversion estimate of the Radon domain, which is expedited by solving multiple, smaller linear systems. Unfortunately, inverse problems are often ill-posed such that uniqueness, existence and stability of the solution are not guaranteed (Tikhonov and Goncharsky, 1987), and RT is no exception (Kuchment, 2006). These concerns are alleviated by the addition of an a priori assumption (regularization). The simplest regularization is based on the ℓ_2 norm (Parker, 1994) of the Radon signal, which is achieved by minimizing the cost function

$$J=\|M(\Delta_j)-\mathbf{A}(\Delta_j,p_i)R(p_i)\|_2^2+\mu\|R(p_i)\|_2^2. \tag{6}$$

The Lagrange multiplier μ determines the trade-off between the least-squares fit of the data (first term in Eq. (6)) and bounding the energy in the Radon domain (second term in Eq. (6)). In our implementation, solutions to linear systems are solved directly, which is sufficient for moderately sized matrices. In the case of large matrices, conjugate gradient methods could be implemented to make computation more feasible.

Regularization methods based on other assumptions include Cauchy-based minimum entropy (Sacchi and Ulrych, 1995) and sparseness approaches associated with the ℓ_1 norm of the Radon signal. However, these regularizations are more computationally expensive since their cost function minimizations are not closed form solutions; instead, iterative methods which converge to the solution are often employed. Earlier solutions to this problem are based on descending the gradient of the cost function (Landweber, 1951). Subsequent algorithms based on proximal gradients (Daubechies et al., 2004) are known for slower convergence rates (sub-linear), though more efficient alternatives have been proposed in recent literature (Bioucas-Dias and Figueiredo, 2007; Beck and Teboulle, 2009). Our inversion code utilizes the Iteratively Reweighted Least Squares (IRLS) method (Daubechies et al., 2010), with linear convergence rates for ℓ_1 norms and quadratic convergence in the limit of ℓ_0 ensures timely computation. The IRLS method assumes a starting model (the ℓ_2 norm solution in our implementation) and updates the Radon solution to the next iteration based on the equation

$$R_{l+1}=(\mathbf{A}^H\mathbf{A}+\lambda\mathbf{Q}_l)^{-1}\mathbf{A}^H M. \tag{7}$$

In Eq. (7) λ is a hyperparameter, $\mathbf{Q}_l$ is a diagonal matrix based on the current Radon solution R_l, $\mathbf{A}^H$ refers to the Hermitian transpose of $\mathbf{A}$ and subscripts refer to the iteration step, with iterations continuing until relative changes to the cost function become negligible. The diagonal entries $Q_{mm}=(|R_m|+b)^{-1}$ and $Q_{mm}=(|R_m|^2+b)^{-1}$ are non-linear due to non-quadratic cost functions for ℓ_1 and Cauchy regularizations, respectively. Within these diagonal elements, a second hyperparameter b has been imposed; this ensures the continuity of the penalty function's gradient and enforces the degree of sparsity in the final solution. The choice of regularization is at the discretion of the researcher depending on, but not limited to, the nature of the application and availability/quality of data.

Optimization of regularization terms is required to ensure fidelity and stability during inversion. If prior information is known about the noise in the spatial domain, then optimization may be achieved through a χ^2 test. This is particularly advantageous for the ℓ_1 and Cauchy inversions as the relationship among μ,λ and b parameters will reduce this problem into the optimization of a single parameter. In the case of real data, little is often known about the noise level and optimization must be achieved empirically based on a trade-off curve (*L*-curve). More

detailed discussions of damping parameter and its optimization can be found in Engl and Grever (1994), Sacchi (1997) and Hansen (1998).

3. Applications

A suite of transverse-component synthetic seismograms is used to demonstrate the effectiveness of RT. Fig. 2A shows a record section of simulated SS precursors (Shearer and Masters, 1992) consisting of ~1000 source-station pairs used in the investigation of mantle stratification beneath South America (Contenti et al., 2012). These synthetics were computed using the reflectivity method based on PREM (Dziewonski and Anderson, 1981) and Global Centroid Moment Tensor solutions (Dziewonski et al., 1981) of the associated earthquakes. Differential times between SS and its precursors provide a proven means for constraining the depths of mantle discontinuities (Shearer and Masters, 1992; An et al., 2007; Gu et al., 2009, see Deuss, 2009 for review).

Each seismogram is aligned on the arrival of the SS surface reflection and sorted according to the epicentral distance. Then, the Radon_inverse routine is applied to the record section (see Fig. 2) while assuming linear path functions in each of the three regularizations: ℓ_2, ℓ_1 and Cauchy. To ensure a fair comparison, we restrict the variance of the residuals (observation-prediction) to a constant value for all regularization approaches. Radon-domain signals are identified for all reflections and the depth errors of the 660, 410 and 220 km discontinuities are less than 0.2%. The emphasis on the sparseness of the solution is apparent in the Cauchy and ℓ_1 Radon solutions; as the most prominent arrival, SS is most significantly affected by the sparseness criterion (Sacchi, 1997).

As suggested by Fig. 2, Radon_inverse constructs the Radon domain and enables accurate assessments of the strength and depth of a given seismic reflection. The opposite operation, Radon_forward, transforms the Radon image back to the spatial domain (Fig. 3). During this process it re-samples SS and its precursors at regular intervals and interpolates phase move-outs within a gap in receiver coverage in the distance range of 110–117° (see Fig. 3). In addition, the ability to mute

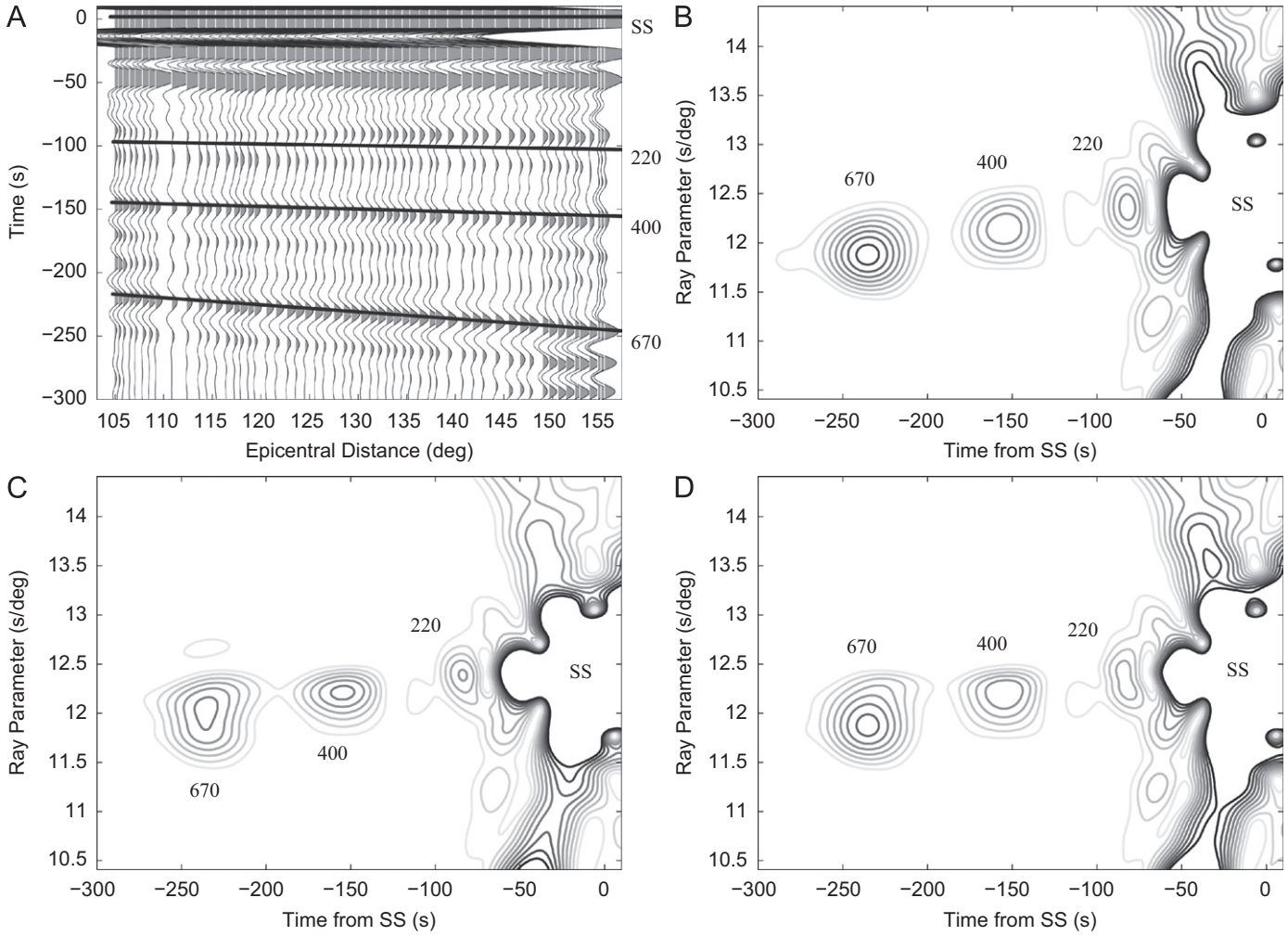

Fig. 2. Radon transform of a simulated record section containing SS and its precursors. (A) SS and its precursors in the spatial domain. The synthetic seismograms have been aligned on SS. Precursors resulting from discontinuities at 220, 410 and 660 km are highlighted by solid lines. The depths of the 410- and 660-km seismic discontinuities are 400 and 670 km, respectively, in PREM. (B) Instantaneous amplitude of the Radon transform, where the inversion was regularized using an L2 norm and $\delta \approx 125$. Distinct peaks in Radon domain are attributed to each ray parameter and their respective slopes in the spatial domain. Additional Radon inversions are performed using (C) ℓ_1 and (D) Cauchy methods. Sharper signals are observed in these two cases, especially for SS, due to the emphasis on sparseness. The variance of the residuals was kept constant to ensure a fair comparison of the inversion methods.

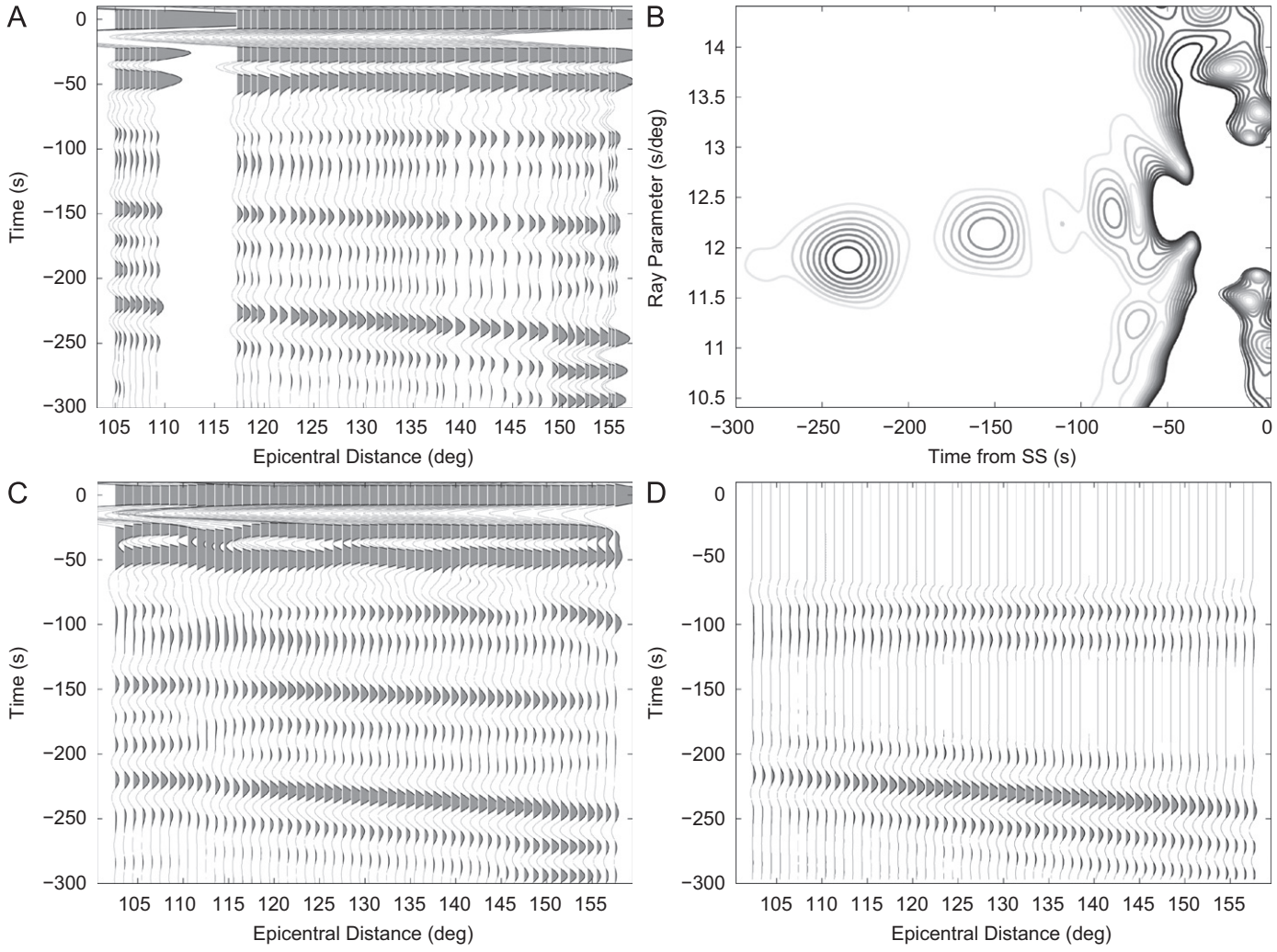

Fig. 3. Resampling and filtering of seismic data using RT. (A) An irregularly sampled synthetic record section containing SS and its precursors. (B) Instantaneous amplitude of RT based on the ℓ_2 regularization. (C) Reconstructed and spatially interpolated record section by applying the forward operator on the Radon signal. (D) Result of applying the forward operator after retaining only the RT signals associated with S220S and S660S.

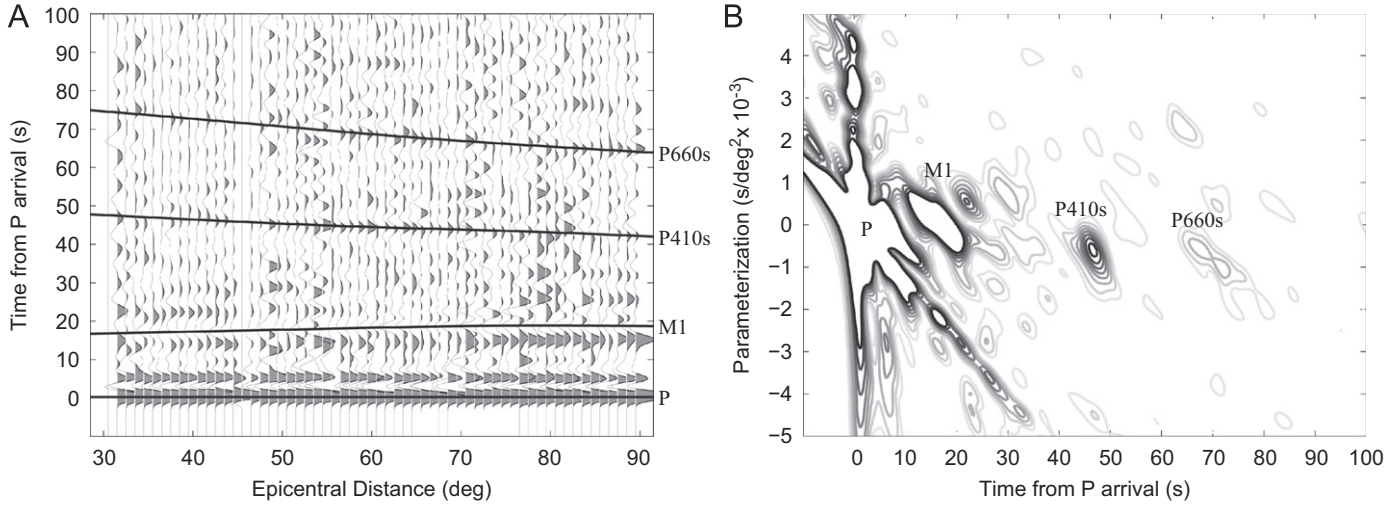

Fig. 4. RT of receiver function data from station EDM. (A) A record section showing nonlinear arrivals originated from crustal multiples and P-to-S conversions at the 410- and 660-km discontinuities. (B) Instantaneous amplitude of RT domain signals. The transform is computed based on the ℓ_2 norm, parabolic path-functions and $\delta = 30$. Signals corresponding to P410s and P660s are recognizable, especially the former due to coherent, energetic arrivals in the spatial domain. A first-order crustal reverberation, near the main P arrival, is labeled M1 in both panels.

other seismic phases greatly facilitates the examination of S220S and S660S in the spatial domain.

The two routines detailed in this study are directly applicable to other geophysical data with a simple change in the input record section (in a matrix form). As an example, we apply RT to radial-component receiver functions (e.g., Langston, 1979; Rondenay, 2009 for review) that were computed based on the broadband seismic data from EDM, a station within the Canadian National Seismic Network. The input record section (Fig. 4A) was obtained using iterative deconvolution (Ligorria and Ammon, 1999) and shows a series of secondary reflected and converted phases after the first arrival. The RT is based on parabolic path functions and an ℓ_2 norm, the preferred modeling choices due to nonlinear move-out curves. Strong signals are observed at the expected times/ray parameters for first-order crustal reverberations and P-to-S conversions from mantle seismic discontinuities (Fig. 4B). Signal corresponding to conversions at the 410-km discontinuity (see Fig. 4B) is best resolved due to coherent time-domain wave amplitudes along the highlighted, de facto move-out curve. The ability to isolate and constrain small, secondary arrivals such as P-to-S conversions in Radon domain could greatly assist the imaging of solid Earth seismic structures.

4. Conclusions

We have presented two Matlab-based routines, Radon_inverse and Radon_forward, that perform discrete inverse and forward Radon transforms. These frequency-based methods offer the user flexible choices among multiple regularization methods and path functions. They are designed for simplicity and flexibility, and the Matlab foundation ensures portability between platforms. Both Radon_inverse and Radon_forward could be readily adapted or modified for a broad range of geophysical applications. The Matlab codes and their instructions are available for download at http://www.ualberta.ca/~rjs10/Software/.

Acknowledgments

We thank Mauricio Sacchi and the Signal Processing Group for their work, which provided valuable information regarding the subject matter. We also thank Natural Resources Canada for making the teleseismic data available. This research is funded by National Science and Engineering Council (NSERC) and the Queen Elizabeth II Graduate Scholarship of the University of Alberta.

Appendix A. Supplementary material

Supplementary data associated with this article can be found in the online version at http://dx.doi.org.10.1016/j.cageo.2012.08.013.

References

An, Y., Gu, Y.J., Sacchi, M., 2007. Imaging mantle discontinuities using least-squares Radon transform. Journal of Geophysical Research 112, B10303.

Beck, A., Teboulle, M., 2009. A fast iterative shrinkage-thresholding algorithm for linear inverse problems. SIAM Journal on Imaging Sciences 2, 183–202.

Beylkin, G., 1987. Discrete Radon transform. IEEE Transactions on Acoustics Speech and Signal Processing 35 (2), 162–172.

Bioucas-Dias, J., Figueiredo, A., 2007. A new TwIST: two-step iterative shrinkage/thresholding algorithms for image restoration. IEEE Transactions on Image Processing 16, 2992–3004.

Bracewell, R.N., 1956. Strip integration in radio astronomy. Australian Journal of Physics 9, 198–201.

Cao, Q., Wang, P., van der Hilst, R.D., de Hoop, M.V., Shim, S.H., 2010. Imaging the upper mantle transition zone with a generalized Radon transform of SS precursors. Physics of the Earth and Planetary Interiors 180, 80–91.

Contenti, S., Gu, Y.J., Okeler, A., Sacchi, M.D., 2012. Shear wave reflectivity imaging of the Nazca-South America subduction zone: stagnant slab in the mantle transition zone?. Geophysical Research Letters 39, L02310.

Cormack, A.M., 1963. Representation of a function by its line integrals, with some radiological applications. Journal of Applied Physics 34, 2722–2727.

Daubechies, I., Defrise, M., Mol, C., 2004. An iterative thresholding algorithm for linear inverse problems with a sparsity constraint. Communications on Pure and Applied Mathematics 41, 909–996.

Daubechies, I., DeVore, R., Fornasier, M., Güntürk, C., 2010. Iteratively re-weighted least squares minimization for sparse recovery. Communications on Pure and Applied Mathematics 63, 1–38.

Deuss, A., 2009. Global observations of mantle discontinuities using SS and PP precursors. Surveys in Geophysics 30, 301–326.

Dziewonski, A.M., Anderson, D.L., 1981. Preliminary reference earth model. Physics of the Earth and Planetary Interiors 25, 297–356.

Dziewonski, A.M., Chou, T.A., Woodhouse, J.H., 1981. Determination of earthquake source parameters from waveform data for studies of global and regional seismicity. Journal of Geophysical Research 86, 2825–2852.

Engl, H.W., Grever, W., 1994. Using the *L*-curve for determining optimal regularization parameters. Numerical Mathematics 69, 25–31.

Gu, Y.J., Sacchi, M., 2009. Radon transform methods and their applications in mapping mantle reflectivity structure. Surveys in Geophysics 30, 327–354.

Gu, Y.J., An, Y., Sacchi, M., Schultz, R., Ritsema, J., 2009. Mantle reflectivity structure beneath oceanic hotspots. Geophysics Journal International 178, 1456–1472.

Hampson, D., 1986. Inverse velocity stacking for multiple elimination. Journal of the Canadian Society of Exploration Geophysicists 22 (1), 44–55.

Hansen, P., 1998. Rank-Deficient and Discrete Ill-posed Problems—Numerical Aspects of Linear Inversions. SIAM.

Horbelt, S., Liebling, M., Unser, M., 2002. Discretization of the Radon transform and of its inverse by spline convolutions. IEEE Transactions on Medical Imaging 21 (4), 363–376.

Kanasewich, E.R., Hemmings, C.D., Aplasian, T., 1973. *N*-th root stack nonlinear multichannel filter. Geophysics 38, 327–338.

Kuchment, P., 2006. Generalized transforms of radon type and their applications. In: Olafsson, G., Quinto, E.T. (Eds.), The Radon Transform, Inverse Problems, and Tomography. American Mathematical Society, Providence, RI, pp. 67–92.

Landweber, L., 1951. An iteration formula for Fredholm integral equations of the first kind. American Journal of Mathematics 73, 615–624.

Langston, C.A., 1979. Structure under Mount Rainier, Washington, inferred from teleseismic body waves. Journal of Geophysical Research 84, 4749–4762.

La Rivière, P.J., Pan, X., 1998. Spline-based inverse Radon transform in two and three dimensions. IEEE Transactions on Nuclear Science 45 (4), 2224–2231.

Ligorria, J.P., Ammon, C.J., 1999. Iterative deconvolution and receiver-function estimation. Bulletin of the Seismological Society of America 89 (5), 1395–1400.

Liu, Q., Gu, Y.J., 2012. Seismic imaging: from classical to adjoint tomography. Tectonophysics 566, 31–66.

Parker, R.L., 1994. Geophysical Inverse Theory. Princeton University Press, Princeton, NJ, 400 pp.

Radon, J., 1917. Über die Bestimmung von Funktionen durch ihre Integralwerte längs gewisser Mannigfaltigkeiten. Berichte über die Verhandlungen der Sächsische Akademie der Wissenschaften 69, 267–277 [in German].

Rondenay, S., 2009. Upper mantle imaging with array recordings of converted and scattered teleseismic waves. Surveys in Geophysics 30, 377–405.

Rost, S., Thomas, C., 2009. Improving seismic resolution through array processing techniques. Surveys in Geophysics 30, 271–299.

Sacchi, M., Ulrych, T.J., 1995. High-resolution velocity gathers and offset space reconstruction. Geophysics 60, 1169–1177.

Sacchi, M.D., 1997. Reweighting strategies in seismic deconvolution. Geophysics Journal International 129, 651–656.

Schimmel, M., Paulssen, H., 1997. Noise reduction and detection of weak, coherent signals through phase-weighted stacks. Geophysics Journal International 130, 497–505.

Shearer, P.M., 1991. Imaging global body-wave phases by stacking long-period SS precursors. Journal of Geophysical Research 96, 20353–20364.

Shearer, P.M., Masters, T.G., 1992. Global mapping of topography on the 660 km discontinuity. Nature 355, 791–796.

Tikhonov, A.N., Goncharsky, A.V., 1987. Ill-Posed Problems in the Natural Sciences. MIR Publisher, Moscow, Russia, 598 pp.

Thorson, J., Claerbout, J., 1985. Velocity-stack and slant-stack stochastic inversion. Geophysics 50, 2727–2741.
Trad, D., Ulrych, T., Sacchi, M.D., 2003. Latest views of the sparse Radon transform. Geophysics 68, 386–399.

Ryan Schultz*, Yu Jeffrey Gu
University of Alberta, Department of Physics, 116 Street and 85 Avenue, Edmonton, Alberta, Canada T6G2G7

E-mail addresses: rjs10@ualberta.ca (R. Schultz), ygu@ualberta.ca (Y. Jeffrey Gu)

Received 29 March 2012

8 August 2012

20 August 2012

* Corresponding author. Tel.: +1 780 318 0404.